QUASI-STEADY FLOW DYNAMICS STUDY OF HUMAN AORTIC VALVE WITH NUMERICAL TECHNIQUES

H.-H. Vu

Department of Mechanical Engineering
National Kaohsiung University of Applied Sciences
Kaohsiung, Taiwan 80778, R.O.C.

C.-H. Hsu *

Department of Mold and Die Engineering
National Kaohsiung University of Applied Sciences
Kaohsiung, Taiwan 80778, R.O.C.

ABSTRACT

Human aortic valve is made of thin collagen type tissue. The three leaflets open and close under fluid forces exerted upon them. To simulate the hemodynamic characteristics of the blood flow, ANSYS CFX10.0 software was utilized to analyze the three-dimensional Reynolds-averaged Navier-Stokes equations. With a quasi-steady analysis model, we predict values of the blood velocity and the wall shear stress both over the valve leaflets and the endothelial lining. In addition, investigation on fluid dynamic of a heart valve supposed suffering prolapsed disease has been also conducted, and compared with normal valve. Analysis results highlight that leaflet opening situation and valve geometry affect the shear stress distribution and vortex flow regime. Maximum shear stress takes place near the center of leaflet trailing edge at the very beginning of systolic phase with value of 7.093N/m^2. At peak systole, the maximum wall shear stress distributes near the aortic root where jet impingement takes place. Current study also demonstrated the interactive impact between low and high wall shear stress on relation to heart valve disease.

Keywords: Aortic valve, Hemodynamic characteristics, Wall shear stress, Prolapsed disease.

1. INTRODUCTION

The viscous drag (shear stress) provided by flowing blood exerts a potent atheroprotective effect [1]. This is evidenced by the finding that atherosclerotic lesions preferentially develop in areas with turbulent flow, whereas regions with uniform laminar flow are protected [2]. The endothelial lining is the primary sensor of wall shear stresses, and functions as a transducer of these biomechanical stimuli into biological responses within the vessel wall [2-4]. The shear stress is highly dependent upon the direction of blood issuing through the orifice of human aortic valve and the location of blood jet impingement. Meanwhile, the orifice shape of aortic valve as well as the location of blood jet impingement could be deformed under influence of valvular diseases. Therefore, it has to consider about effects of heart valve diseases on blood shear stress.

Problems of thrombosis, hemolysis and endothelial lining damage are highly related to hemodynamic analysis of the aortic valves flow regime. Although a number of in vitro techniques are used for studying aortic valve flow and extracting information from the flow [5,6], each has its own special difficulties as well as advantages and each can give only certain data. It is therefore necessary to use several techniques in a complementary manner to gain more aspects of hemodynamic through heart valves. On the other hand, the numerical simulation of flow through heart valves provides an entirely noninvasive method for obtaining quantitative data for velocity and shear stress distributions in the regime. Computational fluid dynamics (CFD) have become popular to determine areas of high fluid stress in the vicinity of heart valves and to improve upon existing artificial valve designs [7]. It is noted that CFD techniques can provide full domain information about flow properties including those yielded by in vitro setup and those cannot. CFD has become a more powerful tool not only for heart valve analysis but also for prosthetic heart valve design with recent improvements in computer hardware and software.

There exists a requirement to setup a three-dimensional numerical model for the analysis to com-

* Corresponding author (chhsu@cc.kuas.edu.tw)

DOI : 10.1017/jmech.2012.105
Copyright © 2012 The Society of Theoretical and Applied Mechanics, R.O.C.
https://doi.org/10.1017/jmech.2012.105 Published online by Cambridge University Press

prehend the complex flow pattern through human aortic valves normal and diseased, for example prior to development and fabrication of a prosthetic valve. This is mainly because that a prosthetic aortic valve with poor geometry design can form a substantial flow obstruction at the ventricle. Since aortic valve geometry affects the flow velocity, it also affects the shear stresses across the leaflets and aortic root. It should be noted that movement of heart valve leaflet is time-dependent, and simulating this kind of displacement is not an easy work. In order to deal with this issue, numerous studies have been conducted by applying quasi-steady approach [8-10]. An important question is raised: Are the quasi-steady leaflet mechanical properties truly representative of their physiological behavior? Fortunately, the reliability of this method applied to valve leaflet problems has been approved experimentally [11].

The present work utilizes a quasi-steady three dimensional CFD model to understand the complex flow pattern through a normal as well as diseased human aortic valve, and concentrates on the analysis of the wall shear stress over the leaflets and endothelial lining.

2. MATERIALS AND METHODS

2.1 Human Aortic Valve Geometry

The valve structure consists of thin flexible sheets (the leaflets) freely suspended between the attachments, forming inter-leaflet seals along the coaptation zone. Swanson and Clark [12] developed an approximate numerical-graphical solution for the motion of a human aortic valve leaflet in a meridional plane through the center of the sinus of valsalva. In this study, we extend the motion to a 3D surface motion model.

The leaflet geometry design in this study is essentially developed by using the partial differential equation (PDE) method [13]. The PDE method generates a surface, $\underline{X}$ in Euclidean 3D space, which is a mapping function of two parameters, for example $\underline{X} = \big(x(u, v), y(u, v), z(u, v)\big)$. The surface is obtained by solving a partial differential equation in parametric *u, v*-space, subject to conditions on the boundary. The PDE may be written as

$$L^{m}_{u,v}(\underline{X}) = 0 \tag{1}$$

Where $L^{m}_{u,v}$ is a partial differential operator of order *m* in the independent variables *u* and *v*.

The method in general is not confined to any particular form of partial differential equation, but so far only elliptic PDEs have been considered, as they produce smooth surfaces for boundary value problems. The order of the PDE is chosen with regard to the number of conditions required of the function and its derivatives at the boundary. In the leaflet considered in the study both function and first derivative conditions are specified on the boundary, so a fourth order PDE is needed. The PDE that generates the surface $\underline{X} = \big(x(u, v), y(u, v), z(u, v)\big)$ is solved separately for each of the *x, y, z* components. Essentially, based on the following PDEs

$$\begin{aligned}
\left(\frac{\partial^2}{\partial u^2} + a^2\frac{\partial^2}{\partial v^2}\right)^2 x = 0 \\
\left(\frac{\partial^2}{\partial u^2} + a^2\frac{\partial^2}{\partial v^2}\right)^2 y = 0 \\
\left(\frac{\partial^2}{\partial u^2} + a^2\frac{\partial^2}{\partial v^2}\right)^2 z = 0
\end{aligned} \tag{2}$$

with conditions

$\underline{X}(u, v)$ specified on the boundary

$\underline{X}_u(u, v)$ or $\underline{X}_v(u, v)$ specified on the boundary

Where '*a*' is a parameter can be interpreted as a smoothing parameter in the sense that it controls the relative smoothing of the dependent variables between the *u* and *v* directions.

Figure 1 shows the coordinate system and boundary conditions for the leaflet model. The *u*, *v*-domain is defined with a region by $0 \le u \le 1$; $0 \le v \le 1$. Here the boundary $u = 0$ and $u = 1$ map to the trailing edge of the leaflet, $v = 0$ maps to the leading edge and $v = 1$ maps to the middle point of the trailing edge. The *x* direction is that of the main blood flow, the *x-z* plane is a meridional plane through the center of the sinus of valsalva. The associated boundary conditions are illustrated in Table 1.

Essentially the leaflet leading edge is designed to be a circular arc with arc angle of $2\pi/3$ radian. A valve shape must be shaped that allows a transition between the valve diameter and the aortic root diameter. This is achieved by using the approximate numerical-graphical solution for the motion of a human aortic valve leaflet in a meridional plane through the center of the sinus of valsalva [12].

Neumann boundary conditions are defined as trigonometric functions with θ measured from the *y* axis in a clockwise direction in the *x-y* plane (refer to Fig. 1) multiplied by the constants K_1, K_2, K_3 and K_4 such that they can be used as interactive parameters to provide quick geometry changes, although the boundary conditions of individual point may be changed as well. The Neumann boundary conditions are defined in the way that the leaflet surface 'leaves' the leading edge boundary ($v = 0$) and 'reaches' the middle of the trailing edge ($v = 1$) through the *x* direction. The tangent vectors around the trailing edge ($u = 0$ and $u = 1$) are defined with a 'smooth' transition from that of along *z* direction at the tip of the leading edge to that of along *x* direction at the middle of the trailing edge by utilizing the trigonometric functions of sinθ, cosθ and sin2θ. The developed leaflet geometry has been confirmed carefully with the dimensions and geometric studies of the human aortic valve of Swanson and Clark [14].

https://doi.org/10.1017/jmech.2012.105 Published online by Cambridge University Press

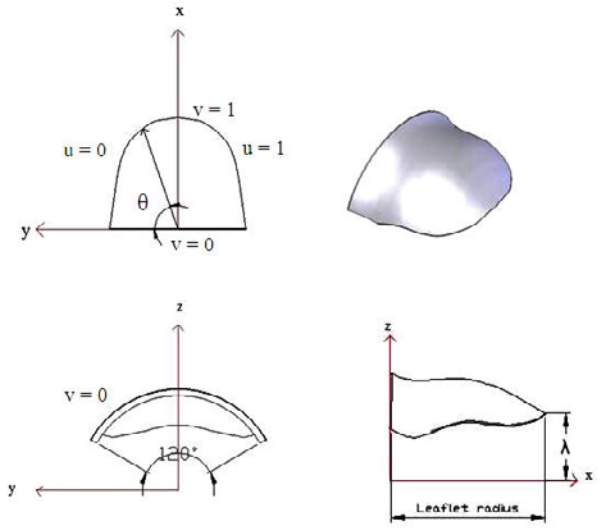


Fig. 1 Coordinate system and boundary conditions for a basic model of a valve leaflet

Table1 Dirichlet and Neumann boundary condition of a valve leaflet design

boundary	Dirichlet boundary condition			Neumann boundary condition		
	x	y	z	x	y	z
$u = 0$	$x^2+y^2=$ (leaflet radius)^2	$x^2+y^2=$ (leaflet radius)^2	approximate numerical-graphical solution [8]	$-K_1\sin\theta$	$-K_1\sin2\theta$	$K_1\cos\theta$
$u = 1$	$x^2+y^2=$ (leaflet radius)^2	$x^2+y^2=$ (leaflet radius)^2	approximate numerical-graphical solution [8]	$-K_2\sin\theta$	$-K_2\sin2\theta$	$K_2\cos\theta$
$v = 0$	0	$y^2+z^2=$ (ventricular tract radius)^2	$y^2+z^2=$ (ventricular tract radius)^2	K_3	0	0
$v = 1$	leaflet radius	0	λ	K_3	0	0

Note: λ is the height above the x axis at the trailing edge center

2.2 Flow Analysis Model

We utilize three-dimensional geometry model to simulate blood flows from the left ventricle through the aortic valve into the aorta.

2.2.1 Governing Equations

To simulate the hemodynamic characteristics of the blood flow, ANSYS CFX10.0 software with the finite volume method of analyzing the three-dimensional Reynolds-averaged Navier-Stokes equations is adopted. Blood is treated as Newtonian fluid with a viscosity of 3.9cP [15]. The governing equations used for present viscous flow-field are Reynolds-averaged equations of Cartesian rectangular coordinate. The tensor forms of the Reynolds-averaged continuity and momentum are as follows:

Continuity equation

$$\frac{\partial}{\partial x_j}(\rho u_j) = 0 \tag{3}$$

Momentum equation

$$\frac{\partial}{\partial x_j}(\rho u_j\, u_i) = -\frac{\partial p}{\partial x_i} + \frac{\partial}{\partial x_j}\left(\mu_{eff}\left(\frac{\partial u_i}{\partial x_j}\right)\right) \tag{4}$$

where

u_i is velocity component in the x_i direction,
p is static pressure,
ρ is fluid density,
μ_{eff} is viscosity ($\mu_{eff} = \mu + \mu_t$; μ is the laminar viscosity; μ_t is the turbulent viscosity).

2.2.2 Turbulent Model

In the present research, the turbulence model proposed by Launder and Spalding [16] is adopted. The k-ε turbulence model along with wall function is employed to solve important parameters including Reynolds stress, turbulent energy flux, and fluctuating viscous work.

In accordance with the k-ε model of Launder and Spalding [16], turbulent viscosity μ_t is represented as follows:

$$\mu_t = \frac{c_\mu\, \rho k^2}{\varepsilon} \tag{5}$$

where k is the turbulent kinetic energy, ε is the dissipation rate of turbulent kinetic energy, and can be individually solved from the equations of turbulent kinetic energy and dissipation rate of turbulent kinetic energy, respectively. Equations of turbulent kinetic energy and dissipation rate of turbulent kinetic energy are listed as bellow.

$$\frac{\partial(\rho u_j\, k)}{\partial x_j} = \frac{\partial}{\partial x_j}\left(\Gamma_k \frac{\partial k}{\partial x_j}\right) + P_k - \rho\varepsilon \tag{6}$$

$$\frac{\partial}{\partial x_j}(\rho u_j\, \varepsilon) = \frac{\partial}{\partial x_j}\left(\Gamma_\varepsilon \frac{\partial \varepsilon}{\partial x_j}\right) + \frac{\varepsilon}{k}(c_{\varepsilon 1}\, P_k - \rho c_{\varepsilon 2}\, \varepsilon) \tag{7}$$

where

$$\Gamma_k = \mu + \frac{\mu_t}{\sigma_k}\ ,\quad \Gamma_\varepsilon = \mu + \frac{\mu_t}{\sigma_\varepsilon}\ ,\quad P_k = \mu_t\left(\frac{\partial u_i}{\partial x_j} + \frac{\partial u_j}{\partial x_i}\right)\frac{\partial u_i}{\partial x_j}$$

standard values of constants of Launder and Spalding [12] are adopted as follows:

$$c_\mu = 0.09\ ,\quad c_{\varepsilon 1} = 1.44\ ,\quad c_{\varepsilon 2} = 1.92\ ,\quad \sigma_k = 1.0\ ,\quad \sigma_\varepsilon = 1.3$$

The no-slip condition or the zero relative velocity between fluid and wall, on the rigid wall is imposed due to the fluid viscosity. The comparative dense grid resolution is usually needed for an accurate prediction inside this region of large velocity gradient. The multi-block grid calculation of ANSYS Workbench 10.0 software is utilized to generate the non-uniform

https://doi.org/10.1017/jmech.2012.105 Published online by Cambridge University Press

grid system. For fewer computational time and data storage consuming, the wall function is adopted for the simulation of near wall flow region with large velocity gradient. The velocity flow field near the wall can thus be accurately predicted using the log-law wall function with fewer grids used.

The finite volume method performs well on the physical conservation and is adopted in the present study. Taking the volume integral on Eqs. (3), (4) and transforming equations into the surface integral forms using Gauss's theorem, the governing equations are as follows.

$$\int_S \rho u_j \, dn_j = 0 \tag{8}$$

$$\int_S \rho u_j \, u_i \, dn_j = -\int_S p dn_i + \int_S \mu_{eff} \left(\frac{\partial u_i}{\partial x_j} + \frac{\partial u_j}{\partial x_i} \right) dn_j \tag{9}$$

Where subscriptions v and s represent the volume and surface integrations respectively, n_j is the outward normal surface vector. Equations (8), (9) are descretized as follows,

$$\sum_{ip} (u_j \, \Delta n_j)_{ip} = 0 \tag{10}$$

$$\sum_{ip} (\rho u_j \, \Delta n_j)_{ip} (u_i)_{ip} = -\sum_{ip} (p \Delta n_i)_{ip} + \sum_{ip} \left(\mu_{eff} \left(\frac{\partial u_i}{\partial x_j} + \frac{\partial u_j}{\partial x_i} \right) \Delta n_j \right)_{ip} \tag{11}$$

Where ΔV is the volume of the control volume, the subscript "*ip*" denotes an integration point, the summation is over all the integration points of the surface and Δn_j is the discrete outward surface vector. The solver used to solve the discritized algebra equations is the Incomplete Lower Upper Factorization Solver with the residuals of 10^{-4}.

2.2.3 Non-Staggered Grid

In solving the incompressible flow field, the solved velocity field may fulfill the continuity equation, which involves no pressure term. However, the pressure oscillation can be observed inconsistent with practical physical phenomena. Two approaches are available to solve the decoupling of pressure and velocity. One of these methods is adopting the staggered grid, which locates the pressure on the node and velocity on the intersection of the surface of the control volume and the gridline. Patankar [17] has addressed this methodology in detail.

In the present study, the decoupling of pressure and velocity is according to the pressure-based fourth order pressure redistribution method and combined with the non-staggered grid. The advantage of using the non-staggered grid is that all required variables locate on the same node, as compared with that by the staggered grid. The same location of both pressure and velocity facilitates that the solution procedure is carried out using definite boundary conditions on cell faces of boundary. Besides, the solution iterations are comparatively decreased for the problem with complex geometries, when the problem arisen from the staggered grid is eliminated [18].

2.2.4 Boundary Conditions

To specify the velocity distribution at the inlet plane is not an easy work since experimental data are not available at this time. To simplify the analysis, we setup a quasi-steady model for the numerical simulation. Any moment during heart beat, the leaflet opening is set along with the associated inflow rate and outlet aortic pressure.

We assume uniform velocity distribution at inlet plane. Only axial velocity is considered and its magnitude is determined to accord with the physiological flow-rate [23]. The physiological state of heart rate 72 beats per minute and stroke volume 70ml is simulated. The peak systole volume flow rate is 380ml per second. The inflow rate and the aortic pressure for the three cases demonstrated in the following sections are shown in Table 2. At the outlet plane, physiological pressure at the moment is specified. No slip and no-flux boundary conditions are imposed on all solid surfaces.

2.2.5 Assumption

According to engineering viewpoint, although human organs, specifically aortic valve, are said to be perfectly non-stop working machines, there is no reason to guarantee a machine could operate forever without fail. Actually, aortic/mitral valve stenosis is such an obvious example for above comment. Heart valve diseases could be due to various reasons from congenital causes to aging, hypertension, *etc*. Valve problem could be stenosis, narrower valve, or insufficiency, leaking valve. Especially, there exists a valve disease rare but still severe namely valve prolapsed. Valve prolapsed is characterized by the displacement of an abnormally thickened valve leaflet, and often found in mitral valves [19]. According to our knowledge, prolapsed disease could also happen to aortic valve.

Within limitation of current research, we assumed that one and two leaflets of aortic valve have problem and moves with different velocity to the others. Case-1 assumed one leaflet to be 0.01sec slower and case-2 with two leaflets being 0.01sec slower.

3. RESULTS AND DISCUSSION

3.1 Physical Models of Human Aortic Heart Valve

We refer the work of King *et al.* [20] and the physical dimensions of ventricle, sinus and aorta are utilized in the study as shown in Fig. 2. The left ventricular entrance radius is 29.50mm and the ventricular tract radius is 13.28mm. The largest radius of sinus is 16.76mm. Aortic exit radius is 14.50mm.

Table 2 Three cases of simulation of the quasi-steady model

	inflow rate (ml/s)	inflow velocity V(m/s)	aortic pressure (mmHg)
case1	50	0.0189	90
case2	175	0.0663	110
case3	290	0.1098	120

https://doi.org/10.1017/jmech.2012.105 Published online by Cambridge University Press

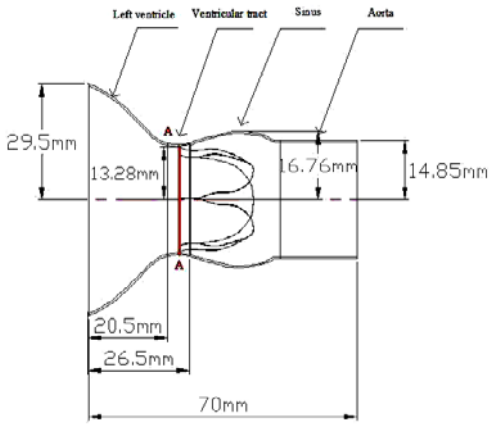


Fig. 2 Physical geometry model

3.2 Flow Field Analysis

ANSYS Work bench 10.0 is utilized to construct the computational mesh and ANSYS CFX10.0 to analyze the flow velocity field and shear stress distribution. In evaluating mesh density accuracy, we choose grid lengths 1.0mm with total 40,380 elements, 1.1mm of 37,522 elements, and 1.2mm of 36,546 elements respectively for the case at peak systole to compare the results. The analysis shows that the flow velocity results are approximately the same. We then compare calculated axial velocity at the A-A section that is located at the ventricular tract (A-A section at Fig. 2). As can be seen in Fig. 3, the calculated speeds are almost the same ('■' for mesh length 1.0mm, '▲' for mesh length 1.1mm and '▼' for mesh length 1.2mm). We therefore adopt mesh density with mesh length 1.0mm as an index in considering the simulation accuracy.

In this research, three cases with different inlet velocity, volume flow rate and leaflet opening are carried out. Here case 1 with the inlet velocity 0.0189m/s and volume flow rate of 50ml/s is the state at very beginning of the systolic phase (the more detailed information of each case is demonstrated in Table 2). Shedding vortex is found between the leaflet and the sinus (Fig. 4(a)). Flow velocity around aortic valve lies between 0.6405m/s and 1.281m/s. The largest velocity distributes around the leaflet trailing edge. It is also the area of violated velocity change happens (Fig. 4(b)).

In case 2, the leaflets are further opening. Flow velocity around aortic valve lies between 0.4872m/s and 0.9742m/s. The largest velocity distributes around the area near the leaflet trailing edge. Trailing edge vortex (Fig. 5(a)) and jet impingement (Fig. 5(b)) have been found for the case. High velocity changes take place in the endothelial lining near the regime of jet impingement. The phenomenon is highly dependent upon the direction of blood issuing through the orifices of the aortic valve.

Case 3 with inlet velocity 0.1098m/s is the state approaching peak systole when volume flow rate of 290ml/s. Flow velocity around aortic valve lies between 0.502m/s and 1.005m/s (Fig. 6). Two areas at

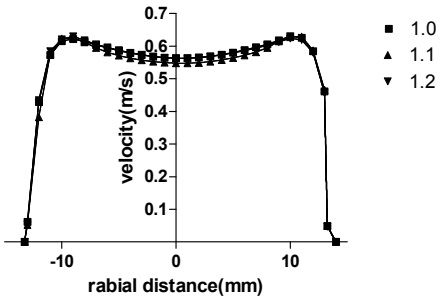


Fig. 3 Calculated Velocity at A-A with different grid lengths

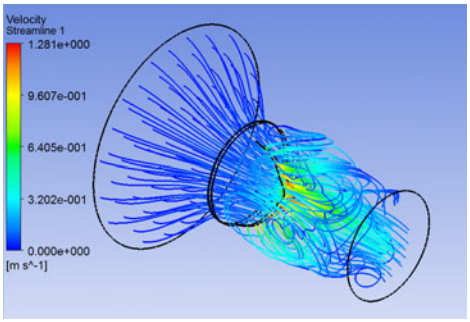


Fig. 4(a) Flow field streak lines at case 1

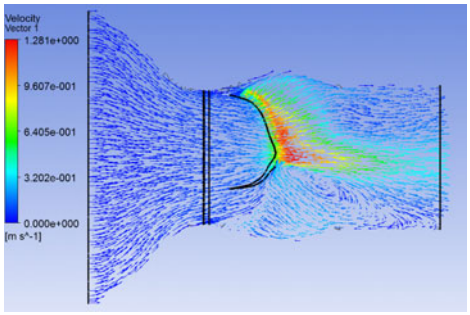


Fig. 4(b) Velocity distribution at *x*-*z* plane for case 1

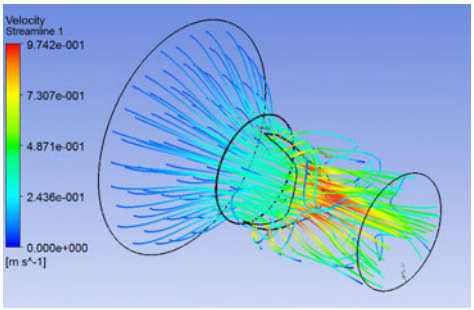


Fig. 5(a) Flow field streak lines at case 2

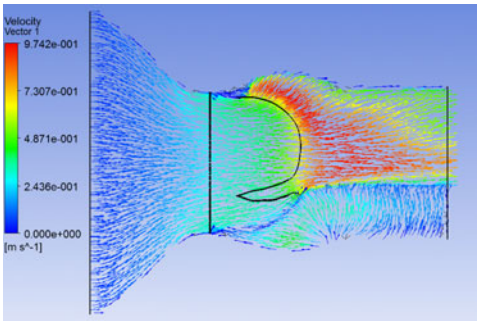


Fig. 5(b) Velocity distribution at *x*-*z* plane for case 2

https://doi.org/10.1017/jmech.2012.105 Published online by Cambridge University Press

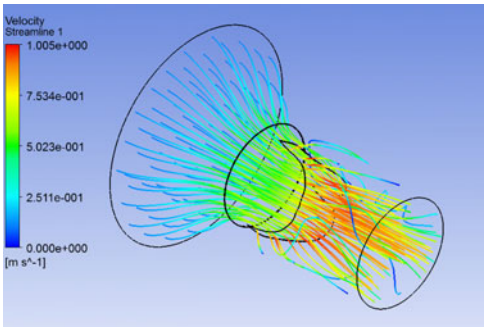


Fig. 6(a) Flow field streak lines at case 3

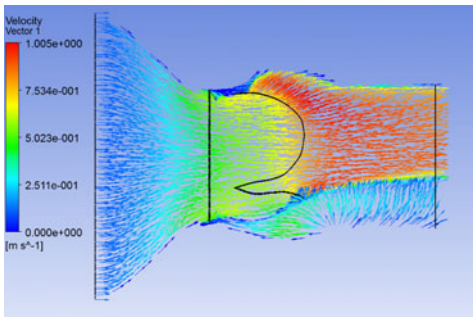


Fig. 6(b) Velocity distribution at *x*-*z* plane for case 3

which large change of velocity happens are that near the jet impingement regime and that near the leaflet trailing edge. These large changes of flow velocity at leaflet trailing edge may induce trailing vortex and lead to the phenomenon of "down-wash" on the leaflet trailing edge. These 'down-wash' velocities tend to induce lift and hence its own moment acting on the leaflet. This provides effect for the leaflet to open.

It is obvious that the leaflet opening/closing affects the variation of flow velocity during a heart beat cycle. When the valve leaflets are in the state of totally opened, the flow field along geometry of the model is relatively smooth. While the obstacle effect increases as the valve leaflets are in the state of initial opening. There exists a recirculation vortex somewhere between the leaflet and the sinus. The blood velocity in this recirculation area is much slower than main flow, which produces lower shear rate, and the flow is almost at rest or stasis regime. The blood cells spirally move inside this vortex, and easily form blood clots. That explains why the thrombosis could be often observed in this area.

On the cardiac cycle, the maximum flow velocity takes place somewhere near the central orifice among the three leaflets. Blood flow owns dramatic changes in velocity and shear stress for all the cases in the central entrance regime. As blood flows toward the leading edge of the leaflet, the pressure in the fluid particle rises from the free stream pressure to the stagnation pressure. The high fluid pressure near the leading edge impels the developing boundary layer. However, the pressure force is not sufficient to force the boundary layer around the back side of the leaflet at high Reynolds numbers.

Since the pressure increases in the direction of flow, the fluid elements experience a net pressure force opposite to its direction of motion. At some point around the leaflet the movement of the fluid in the boundary layer is insufficient to carry the element further into to the region of increasing pressure. The fluid layer adjacent to the solid surface will be brought to rest and the flow will separate from the surface. The boundary layer separation forms shear layer that trails aft in the flow and bounds the wake.

Since the innermost portion of the free shear layer moves much more slowly than the outermost portion of the layer which is in contact with the free stream, the free shear layer tends to roll up into discrete, swirling, vortices. A regular pattern of vortices is formed in the wake that interacts with the leaflet motion and is the source of the effects called vortex-induced vibration. As the flow velocity is increased or decreased so that the vortex shedding frequency approaches the natural frequency of the structure, the vortex shedding suddenly locks into the structure frequency. The lock-in resonant oscillation of the near wake, input energy to the structure so that large amplitude vibrations can be produced. This mechanism would induce the fluttering motion when the leaflets are at the fully open position.

3.3 Wall Shear Stress Analysis

Flow field analyses of the aortic valve pointed out the corresponding velocity distribution trends and changes at different leaflet opening. Once the leaflets begin to open, shedding vortex appears obviously right behind the leaflets (Fig. 4). These vortexes affect the factors on blood coagulation. Once the leaflets completely open, the distribution of the flow field is smooth and the flow roughly along the wall geometric appearance. Pressure near leaflet under surface is greater than that near the upper surface. This leads flow rolling up and forms a trailing vortex (Fig. 6). Blood flow velocity changes dramatically for the location of leaflet trailing edge and sinus wall where the jet impingement happens.

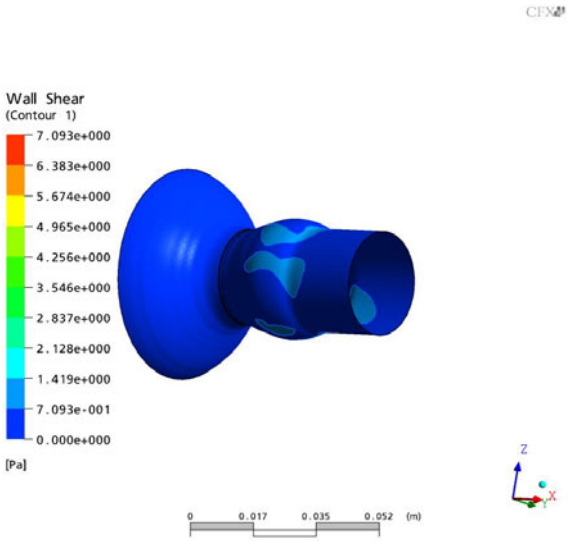
Figure 7 shows wall shear stress of aortic root at systolic phases for the case 1, 2 and 3. Figure 8 shows the wall shear stress around the leaflet surface. Wall shear stress is the tangential stress acting on the surface. The wall shear stress is given by [21]:

$$\tau_w = \mu_{eff}(du/dr) \tag{12}$$

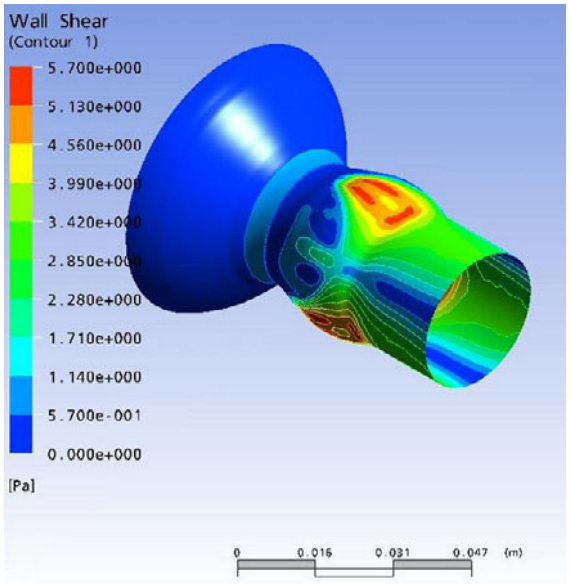
Here $\mu_{\text{eff}} = \mu + \mu_t$ is the effective viscosity; du/dr is gradient of tangential velocity u, in the normal direction r. The maximum wall shear stress of the aortic root distributes somewhere near the jet impingement.

At very beginning of the systolic phase, the maximum shear stress is around 7.093N/m^2 and locates somewhere near the center of leaflet trailing edge (Fig. 8). The location of the maximum shear stress area shifts to endothelial lining area of jet impingement (Fig. 7) as leaflet further opening. The maximum shear stress is 5.7N/m^2 for case2 and 5.93N/m^2 for case3. In view of the shear stress value, the possibility of endothelial lining damage which occur at shear stress around 40N/m^2 [22] will be very low for the human aortic valve.

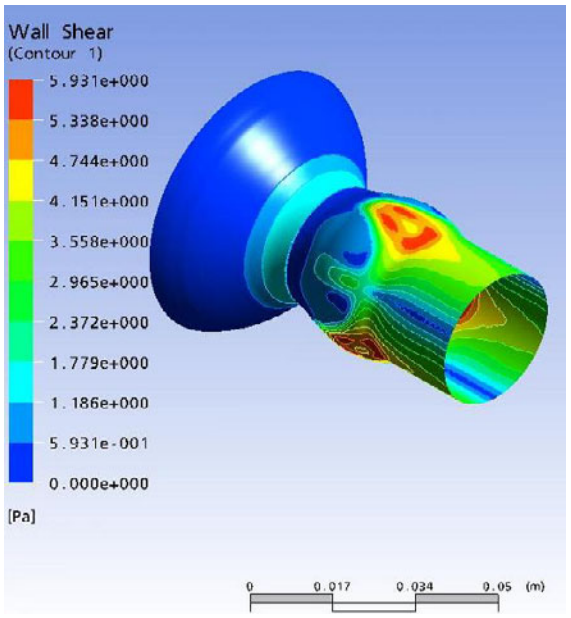
https://doi.org/10.1017/jmech.2012.105 Published online by Cambridge University Press



(a) Case 1

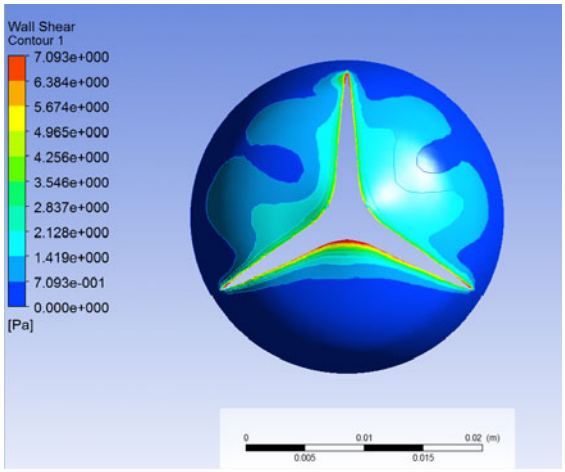


(b) Case 2

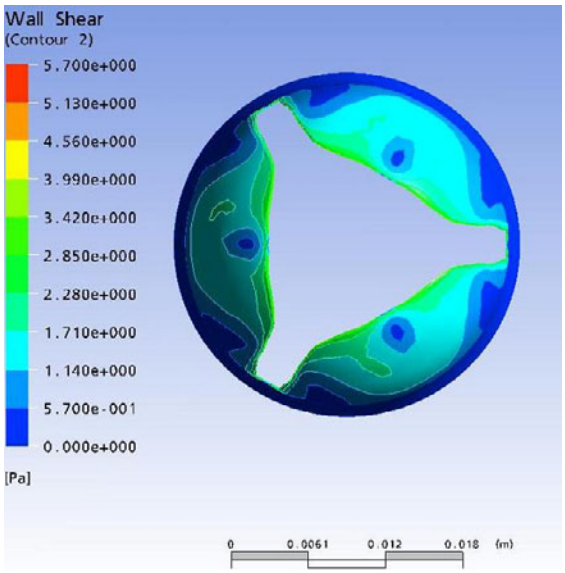


(c) Case 3

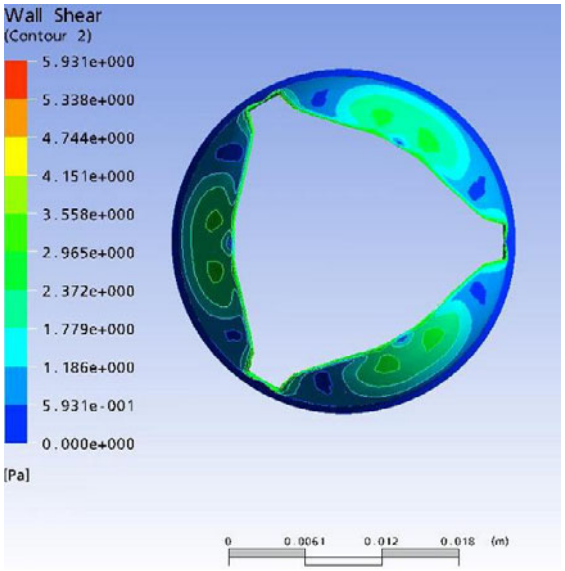
Fig. 7 wall shear stress of aortic root at systolic phases



(a) Case 1



(b) Case 2

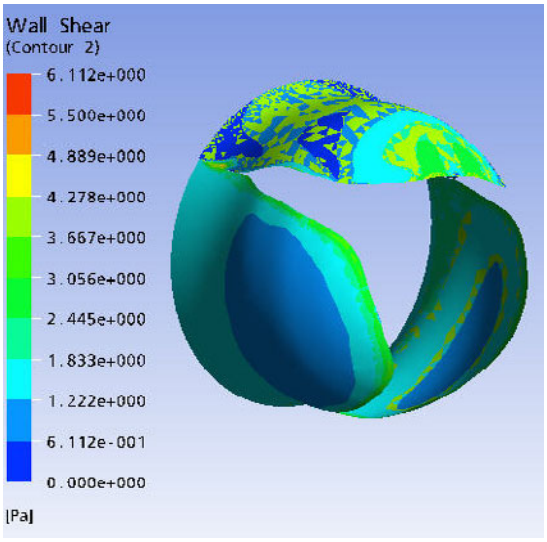


(c) Case 3

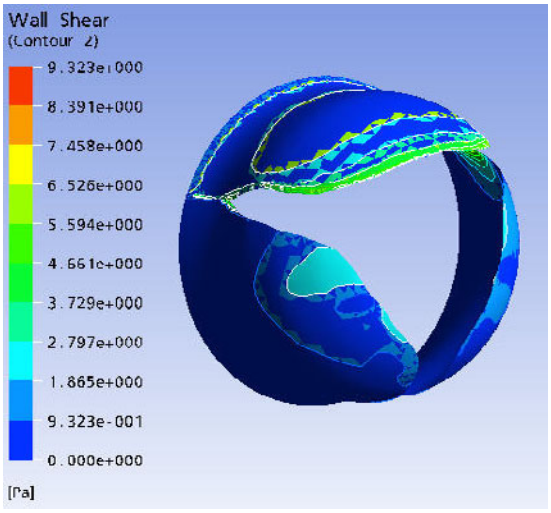
Fig. 8 wall shear stress of leaflet surface at systolic phases

https://doi.org/10.1017/jmech.2012.105 Published online by Cambridge University Press

Theoretically, damage of endothelial lining by high shear stress could lead to sclerosis in valve leaflet, and results in abnormally thickened leaflet. In contrast, low wall shear stress is also considered as a main factor causes sclerosis, low wall shear stress theory [23]. The low wall shear stresses impair mass transport between blood and the vessel/valve leaflet wall, potentially impacting on not only the uptake of nutrients and oxygen by the vessel/valve leaflet wall from the blood, but also the release of waste products and carbon dioxide into the blood from the wall. This latter effect would help explain how material components typically found in atherosclerotic lesions and plaques may build up in the vessel/valve leaflet wall with slow or stagnant flow. The simulation results of natural heart valve above show that the found maximum wall shear stress is far from the damage limit of endothelial lining. However, this low shear stress combined with shedding vortices appears between tip of valve leaflet and sinus could induce sclerosis in valve leaflet, thus lead to exceptional displacement of leaflet namely prolapsed disease. Current work assumed two cases of disease could happen to valve leaflet including one leaflet moving 0.01second slower, and two leaflets moving 0.01seccond slower. The inlet was set to the state approaching peak systole when flow rate was 290mml/s. For the case of one failed leaflet, the maximum wall shear stress is found as 6.112N/m^2 (Fig. 9(a)), while this value is 9.323N/m^2 for the case of two failed leaflets (Fig. 9(b)). For both two cases, the maximum wall shear stress increased 3% and 57%, respectively compared with normal valve. Especially, the wall shear stress found in case of two failed leaflets is even higher than that of normal valve at beginning of systolic phase. Although this value is still far from damage limit of endothelial lining, the simulation results have illustrated the complex flow of diseased heart valve with unpredictable phenomenon.



(a) One failed leaflet



(b) Two failed leaflets

Fig. 9 wall shear stress of leaflet of prolapsed heart valve at systolic phases

4. CONCLUSIONS

In this study, computational fluid dynamics is utilized to simulate the blood flow velocity and shear stress through aortic valve in normal and prolapsed states with different opening situation by a quasi-steady numerical model.

Although the validity of quasi-steady method has been experimentally proved [11], the time-dependent movement of heart valve leaflet can only be completely solved by methods that associated with fluid-structure interaction (FSI) problems. However, these methods cost much of calculation efforts, complicated algorithms, and hardware expenses. Therefore, the computing models using these methods often need to be simplified or utilize the symmetry to reduce the calculation. These constraints are really disadvantages of the methods when problems require using more realistic models that are often asymmetry, or need to deal with valves with diseases which often result in asynchronous movement of valve leaflets. Some studies [24,25] have made efforts to investigate problems of heart valves with diseases, but an insightful result including both flow field and shear stress analysis has not been yet provided. Contrastingly, quasi-steady method can apply to most of problems with complicated simulating models, but costs less calculating time and simple algorithm. Due to the advantages of quasi-steady method, this method has been selected in current study, and we can get some conclusions from the results as following:

1. During a heart beat cycle, the leaflet opening/closing affects the variation of flow velocity. Especially, the appearance of the recirculation vortex could be observed somewhere between the leaflet and the sinus when the valve leaflets are in the state of initial opening, which could produce a lower shear rate at which blood clots could form.
2. On the cardiac cycle, the maximum flow velocity takes place somewhere near the central orifice among the three leaflets. Blood flow owns dramatic changes in velocity in the central entrance regime, which may lead to a phenomenon called “down-wash” that generates a lift effect on valve leaflets.

https://doi.org/10.1017/jmech.2012.105 Published online by Cambridge University Press

3. A regular pattern of vortices is formed in the wake that interacts with the leaflet motion and is the source of the effects called vortex-induced vibration. This mechanism would induce the fluttering motion when the leaflets are at the fully open position.
4. The largest shear stress happens in the endothelial lining where jet impingement takes place. The jet impingement is highly dependent on the opening of the leaflets. The phenomena are obvious when the opening angle increases. While the induced shear stress is not big enough to damage endothelial lining.
5. The interactive relation between low and high wall shear stress has been demonstrated in this study. Low wall shear stress acting on valve leaflet could lead to a valvular disease somehow. This disease in contrast induces higher shear stress, and thus, makes the disease become worse.

ACKNOWLEDGEMENTS

This work was supported by National Science Council research project of grand number NSC94-2614-E-218-001.

REFERENCES

1. Gimbrone, M. A., Nagel, T. and Topper, J. N., "Biomechanical Activation: An Emerging Paradigm in Endothelial Adhesion Biology," *Journal of Clinical Investigation*, **99**, pp. 1809–1813 (1997).
2. Gimbrone, M. A., Topper, J. N., Nagel, T., Anderson, K. R. and Garcia-Cardena, G., "Endothelial Dysfunction, Hemodynamic Forces, and Atherogenesis," *Annals of the New York Academy of Sciences*, **902**, pp. 230–240 (2000).
3. Traub, O. and Berk, B. C., "Laminar Shear Stress: Mechanisms by Which Endothelial Cells Transduce an Atheroprotective Force," *Arteriosclerosis, Thrombosis and Vascular Biology*, **18**, pp. 677–685 (1998).
4. Chien, S., Li, S. and Shyy, Y. J., "Effects of Mechanical Forces on Signal Transduction and Gene Expression in Endothelial Cells," *Hypertension*, **31**, pp. 162–169 (1998).
5. Akutsu, T. and Saito, J., "Dynamic Particle Image Velocimetry Flow Analysis of the Flow Field Immediately Downstream of Bileaflet Mechanical Mitral Prostheses," *Journal of Artificial Organs*, **9**, pp. 165–178 (2006).
6. Lee, H., Tatsumi, E., Homma, A., Tsukiya, T. and Taenaka, Y., "Mechanism for Cavitation of Monoleaflet and Bileaflet Valves in an Artificial Heart," *Journal of Artificial Organs*, **9**, pp. 154–160 (2006).
7. Ge, L., Jones, S. C., Sotiropoulos, F., Healy, T. M. and Yoganathan, A. P., "Numerical Simulation of Flow in Mechanical Heart Valves: Grid Resolution and the Assumption of Flow Symmetry," *ASME Transaction: Journal of Biomechanical Engineering*, **125**, pp. 709–718 (2003).
8. Kortsmit, J., Driessen, N. J. B., Rutten, M. C. M. and Baaijens, F. P. T., "Real Time, Non-Invasive Assessment of Leaflet Deformation in Heart Valve Tissue Engineering," *Annals of Biomedical Engineering*, **37**, pp. 532–541 (2009).
9. Sun, W., Abad, A. and Sacks, M. S., "Simulated Bioprosthetic Heart Valve Deformation Under Quasi-Static Loading," *ASME: Journal of Biomechanical Engineering*, **127**, pp. 905–914 (2005).
10. Haj-Ali, R., Dasi, L. P., Kim, H. S., Choi, J., Leo, H. W. and Yoganathan, A. P., "Structural Simulations of Prosthetic Tri-Leaflet Aortic Heart Valves," *Journal of Biomechanics*, **41**, pp. 1510–1519 (2008).
11. Sacks, M. S. and Yoganathan, A. P., "Heart Valve Function: A Biomechanical Perspective," *Philosophy Transactions of the Royal Society B*, **362**, pp. 1369–1391 (2007).
12. Swanson, W. M. and Clark, R. E., "Aortic Valve Leaflet Motion During Systole," *Circulation Research*, **32**, pp. 42–48 (1973).
13. Hsu, C. H., "A Visualization Design Environment for Quick Designs of Prosthetic Mechanical Heart Valves," *Ph.D. Thesis, Department of Mechanical Engineering, Leeds University*, U.K. (1995).
14. Swanson, W. M. and Clark, R. E., "Dimensions and Geometric Relationships of the Human Aortic Value as a Function of Pressure," *Circulation Research*, **35**, pp. 871–882 (1974).
15. Walker, P. G. and Yoganathan, A. P., "In Vitro Pulsatile Flow Hemodynamics of Five Mechanical Aortic Heart Valve Prostheses," *European Journal of Cardio-thoracic Surgery*, **6**, pp. s113–123 (1992).
16. Launder, B. E. and Spalding, D. B., "The Numerical Computation of Turbulent Flows," *Computer Methods in Applied Mechanics and Engineering*, **3**, pp. 269–289 (1974).
17. Patankar, S. V., *Numerical Heat Transfer*, Hemisphere, Washington, D.C. (1980).
18. Prakash, C. and Patankar, S. V., "A Control Volume Based Finite Element Method for Solving the Navier-Stokes Equations Using Equal Order Velocity-Pressure Interpolation," *Numerical Heat Transfer*, **8**, pp. 259–280 (1985).
19. ACC/AHA Pocket Guideline, "Management of Patients with Valvular Heart Disease," *American College of Cardiology Foundation*, American Heart Association, Inc, pp. 17–18 (2006).
20. King, M., David, T. and Fisher, J., "An Initial Parametric Study on Fluid Flow Through Bileaflet Mechanical Heart Valves, Using Computational Fluid Dynamics," *Journal of Engineering in Medicine*, **208**, pp. 63–72 (1994).
21. Yoganathan, A. P., Woo, Y. R. and Hsing, W. S., "Turbulent Shear Stress Measurements in the Vicinity of Aortic Valve Prostheses," *Journal of Biomechanics*,

https://doi.org/10.1017/jmech.2012.105 Published online by Cambridge University Press

19, pp. 433–442 (1986).
22. Fry, D. L., "Acute Vascular Endothelial Changes Associated with Increased Blood Velocity Gradients", *Circulation Research*, **12**, pp. 165–197 (1968).
23. Chandran, K. B., Yoganathan, A. P. and Rittgers, S. E., *Biofluid Mechanics – The Human Circulation*, Taylor & Francis Group, LLC (2007).
24. Van Loon, R., "Towards Computational Modeling of Aortic Stenosis," *International Journal of Numerical Methods Biomedical Engineering*, **26**, pp. 405–420 (2010).
25. Korakianitis, T. and Shi, Y., "Numerical Simulation of Cardiovascular Dynamics with Healthy and Diseased Heart Valve," *Journal of Biomechanical*, **39**, pp. 1964–1982 (2006).

(Manuscript received September 15, 2011,
accepted for publication March 14, 2012.)

https://doi.org/10.1017/jmech.2012.105 Published online by Cambridge University Press